BMC Pediatrics

RESEARCH Open Access

A novel missense variant at the site of interaction between RLIM and E2 ubiquitin-conjugating enzymes causes Tønne-Kalscheuer syndrome

Evelina Siavrienė[1*], Justas Dapkūnas[2], Živilė Maldžienė[1], Violeta Mikštienė[1], Gunda Petraitytė[1] and Eglė Preikšaitienė[1]

Abstract

Hemizygous variants in the *RLIM* gene, which is located on chromosome Xq13, cause Tønne-Kalscheuer syndrome (TOKAS). This X-linked recessive disorder is characterized by intellectual disability (ID), global developmental delay, behavioral impairment, gait disturbances, minor facial anomalies, congenital diaphragmatic hernia, skeletal and urogenital abnormalities, including hypogenitalism, micropenis, and cryptorchidism. In this study, we report on a novel, likely pathogenic *RLIM* variant in a proband, the clinical phenotype of which is consistent with a diagnosis of TOKAS.

Whole-exome sequencing (WES) was performed on a genomic DNA (gDNA) sample of the proband to identify the disease-causing variant. Validation and segregation analysis were performed by Sanger sequencing of the proband's and his mother's gDNA samples. Computational analysis and protein structure modelling were applied to assess the possible influence of the variant on protein function.

A novel missense variant NM_016120.4:c.1721T > A, NP_057204.2:p.(Ile574Asn) in the *RLIM* gene was identified by the analysis of WES data. Segregation analysis revealed the asymptomatic mother to be a carrier of the familial missense variant, and a highly skewed X chromosome inactivation pattern was observed in this study. The altered residue was determined to be at the interaction interface between E3 ubiquitin ligase RLIM and E2 ubiquitin-conjugating enzymes.

The findings provided in this study suggest that the affected residue Ile574 could alter the interactions of the RING domain with the E2 ubiquitin-conjugating enzymes and therefore could influence the ubiquitin-mediated protein regulation pathways.

Keywords RLIM, Tønne-Kalscheuer syndrome, X-linked intellectual disability, Missense variant

*Correspondence:
Evelina Siavrienė
evelina.siavriene@mf.vu.lt
[1]Department of Human and Medical Genetics, Institute of Biomedical Sciences, Faculty of Medicine, Vilnius University, Vilnius, Lithuania
[2]Department of Bioinformatics, Institute of Biotechnology, Life Sciences Center, Vilnius University, Vilnius, Lithuania

Introduction

The human X chromosome accounts for about 5% of the human genome and contains more than 1,000 different genes. More than 160 genes have been reported to be associated with X-linked intellectual disability. The number of newly identified XLID genes is still growing due to rapid technological advancements [1, 2].

Pathogenic variants in the *RLIM* (MIM 300379) gene, also known as *RNF12*, lead to syndromic XLID. Disease-causing variants in *RLIM* were first reported in 2015 [3]. E. Tønne et al. described a three-generation Norwegian family with four affected individuals [3], while a research group led by V. Kalscheuer reported three unrelated families with pathogenic variants in *RLIM* in a simultaneous publication [4]. The newly described Tønne-Kalscheuer syndrome (TOKAS, MIM 300978) has since been diagnosed in additional families. To date, nearly 20 unrelated families have been reported in the literature [3–9].

Despite the growing number of families with disease-causing *RLIM* variants, the clinical recognition of the syndrome is still challenging due to the broad phenotypic spectrum of intellectual disability syndromes. TOKAS shows phenotypic overlap with several other genetic conditions, particularly Fryns syndrome (MIM 229850), which is caused by homozygous or compound heterozygous variants in the *PIGN* (MIM 606097) gene [5, 10]. Additionally, some clinical features are shared with Donnai-Barrow (MIM 222448), Matthew-Wood (MIM 601186), Simpson-Golabi-Behmel (MIM 312870), CHARGE (MIM 214800), Cornelia de Lange (MIM 122470), Smith-Lemli-Opitz (MIM 270400), Wolf-Hirschhorn (MIM 194190), and microphthalmia, dermal aplasia, and sclerocornea (MIDAS; MIM 309801). Many of these syndromes present with varying degrees of intellectual disability and may have other characteristics such as dysmorphic facial features, congenital diaphragmatic hernia (CDH), and differences in sex development (DSD). While these conditions share a degree of phenotypic overlap, the specific combination of intellectual disability, multi-systemic anomalies (e.g., speech delay, behavioral impairment, growth retardation, gait disturbances, microcephaly, skeletal anomalies, CHD), and a characteristic pattern of DSD in males serves as a key distinguishing feature of TOKAS. Also, the syndrome has been described as clinically recognisable by such characteristic facial features as a broad, prominent, or high forehead, a broad or high nasal bridge, hypertelorism, straight eyebrows, synophrys, facial asymmetry, thin upper lip, malar hypoplasia, downturned corners of the mouth, open-mouthed appearance, small pointed chin, micrognathia, and widely spaced teeth [3–6, 8]. Although the clinical features of TOKAS are well-defined, the definitive diagnosis relies on the unique combination of these features and is ultimately confirmed by the identification of a pathogenic variant in the *RLIM* gene.

RLIM encodes an E3 ubiquitin ligase that contains a RING-H2 domain, which mediates ubiquitin-dependent protein degradation and regulates transcriptional activity. This function is critical for embryonic development, including X-chromosome inactivation, organogenesis, and neuronal differentiation. Pathogenic variants affecting the RING ubiquitin ligase activity, thereby disrupting these essential developmental pathways and contributing to the molecular pathogenesis of TOKAS. In this study, we report on a Lithuanian family with a novel, likely pathogenic, familial variant in the RLIM C-terminal catalytic RING-H2 zinc finger domain, resulting in possible alterations of the ubiquitin-mediated protein degradation pathway and thus causing TOKAS.

Materials and methods

DNA extraction

Genomic DNA (gDNA) was isolated from peripheral blood leukocytes of the proband and his mother using the phenol-chloroform-isoamyl alcohol extraction method [11].

Whole-exome sequencing

Whole-exome sequencing (WES) was performed by CeGaT (Tübingen, Germany) to sequence the DNA sample of the proband. Sequencing libraries were created according to the manufacturer's guidelines using the Twist Human Core Exome Kit, the RefSeq, and the Mitochondrial Panel (Twist Bioscience, San Francisco, CA, USA). The high-throughput next-generation NovaSeq 6000 (Illumina Inc., San Diego, USA) platform was used for sequencing with 2 × 100 base pairs (bp) read length. WES data were processed with Illumina bcl2fastq (2.20). Adapters were trimmed with Skewer v0.2.2 [12].

The raw sequences were aligned to the human reference genome (GRCh37/hg19) using the Burrows-Wheeler Aligner (BWA-mem v0.7.17) [13]. The data annotation was made using the ANNOVAR v2018 Apr16 [14]. Guidelines and recommendations provided by the American College of Human Genetics and Genomics (ACMG) [15], in silico tools and databases provided by ANNOVAR (e.g., SIFT, Polyphen2, GERP++, CADD, ExAC v0.3.1, GnomAD v4.1.0, 1000 Genome Project data v1000g2015aug_all, Kaviar Genomic Variant v160204-Public, Database NCBI dbSNP, NCBI ClinVar), and the scientific literature were used to assess the pathogenicity of detected variants. The candidate genome variants were checked and validated by the Integrative Genomics Viewer (IGV) visualization tool [16].

Sanger sequencing

Sanger sequencing was performed on gDNA from the proband and his mother to validate the WES findings and assess variant segregation in the family. gDNA samples from the father and affected brother were unavailable for this analysis.

Polymerase chain reaction (PCR) of gDNA sequences flanking the possibly disease-causative variant of the *RLIM* gene was performed using specific primers (Supplementary Table S1) designed with the Primer Blast tool. PCR was performed using Phusion High-Fidelity PCR Master Mix (Thermo Fisher Scientific, USA). PCR products were fractioned by 1.5% agarose gel (TopVision, Thermo Fisher Scientific, USA) electrophoresis and visualized under ultraviolet light.

S equence analysis of the PCR product was carried out with BigDye® Terminator v3.1 Cycle Sequencing Kit (Thermo Fisher Scientific, USA) on an ABI 3130xL Genetic Analyser (Thermo Fisher Scientific, USA). The resulting sequences were aligned with the reference sequence of *RLIM* (NCBI: NM_016120.4).

X chromosome inactivation

X-chromosome inactivation analysis of gDNA extracted from the blood was performed using methylation-sensitive fragment analysis of a polymorphic CAG repeat in the first exon of the androgen receptor (*AR*) gene. gDNA of the proband, his mother, and female controls were amplified with a fluorescently labeled forward primer and an unlabeled reverse primer flanking the polymorphic CAG repeat before and after HpaII digestion. The primer sequences and the PCR conditions have been described previously [17]. Subsequently, we subjected the PCR products to the ABI 3130xl (Applied Biosystems, Foster City, CA, USA) and evaluated the heights of peaks of PCR products using GeneMapper Analysis software (v3.7; Applied Biosystems, Foster City, CA, USA). The X-chromosome inactivation (XCI) ratio was calculated by dividing the heights of peaks of PCR products using gDNA treated with HpaII by those of PCR products using gDNA treated without HpaII. An XCI ratio of 80% or more was regarded as a skewed XCI based on criteria provided by Bertelsen et al. (2011) [18].

In Silico predictions

Sequences of RLIM (UniProt AC: Q9NVW2) and other proteins were obtained from the UniProt database [19], and the RLIM structure model was downloaded from the AlphaFold Database [20]. Experimental structural data on protein-protein interactions were analyzed in the PPI3D server [21]. Structures of RLIM-E2 complexes were predicted using AlphaFold-Multimer (v2.3, "full_dbs" preset, no templates) [22, 23]. The accuracy self-estimation of the top-ranked AlphaFold models is provided in Supplementary Table S2. Structures and structure models were analyzed using Voronota [24] and HBplus software [25], as well as in the VoroContacts server [26]. Disordered regions were predicted using DISOPRED3 [27].

The data on interactions between RLIM and E2 ubiquitin conjugating enzymes were taken from Bustos et al. (2018) [28]. Multiple sequence alignment of human E2 proteins was generated using MAFFT with l-INS-i option [29]. Alignment was visualized using JAlview [30]. Sequence logos were generated using the WebLogo 3 server [31]. The influence of variants was checked in the AlphaMissense predictions database [32].

Results

Clinical evaluation

The proband (III-1)

The 7-year-old proband, a male, was the first child of healthy, unrelated Lithuanian parents aged 23 (mother) and 28 (father) at the proband's birth (Fig. 1A). The proband was born from the first pregnancy, which was complicated by imminent preterm labour at 32 weeks of gestation. The proband was born at full term by a Caesarean section due to prolonged labour. His birth weight was 3.430 g (25th centile), his length was 52 cm (25th centile), and his Apgar score at 1 min was 10. Strabismus and cryptorchidism on the right side were observed

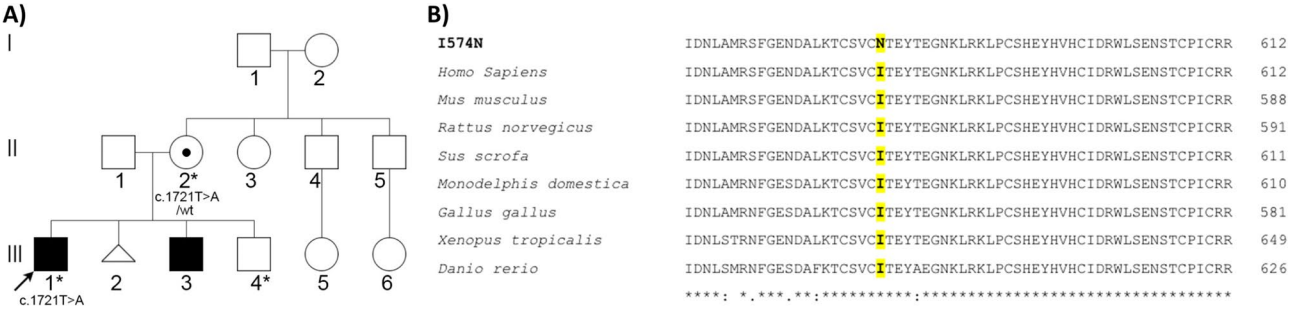

Fig. 1 (**A**) Genealogy of the family. The arrow shows a proband. The black symbol shows affected individuals. * indicates tested individuals. (**B**) Multiple-sequence alignment of the RLIM protein across eight evolutionarily distant species. Substitution p.(Ile574Asn) is highlighted in yellow. Below the amino acid sequences is a key denoting conserved sequence (*), conservative variants (:), semi-conservative variants (.), and non-conservative ()

after birth. The neonatal period was complicated by feeding problems. Mild eczema manifested at the age of 4–6 months. Eyeglasses for the correction of a refraction error and strabismus were prescribed at 9 months of age. Surgical correction of cryptorchidism was performed at the age of 11 months. At the age of 7 years, hypothyroidism was diagnosed, and treatment with levothyroxine was started. At this age, the proband was also hospitalised at the paediatric neurology department due to suspicion of paroxysmal clinical events and trouble sleeping. Neurological evaluation showed dysarthria, dysphasia, strabismus, impaired fine and gross motor skills, mild hypotonia, and no changes in gait or coordination. Epileptiform activity was not recorded in the EEG during sleep. Abdominal and renal ultrasound examination showed an accessory spleen and no other significant abnormalities. In addition to ultrasound, the chest X-ray was normal and did not reveal a congenital diaphragmatic hernia. The proband has been followed by a paediatric neurologist for global developmental delay since infancy. He could stand with support at 12 months, walk independently at 19 months, and speak his first words at the age of 3 years. The proband had fears of loud sounds and closed spaces. At the age of 4 years, his psychomotor development was evaluated according to the DISC scale: gross motor skills – 23 months, fine motor skills – 24 months, language perception – 24 months, language expression – 14 months, auditory attention and memory – 18 months, visual attention and memory – 21 months, independence – 29 months, and social adaptation – 27 months. His psychological evaluation at the age of 8½ years yielded a verbal scale of 51, a performance of 47, and a full scale of 45 on the Wechsler Intelligence Scale for Children (WISC-III). The proband had avoidant/restrictive food intake disorder, poor weight and height growth, and a tendency to constipation. On examination at the age of 7 years, his head circumference was 52 cm (25th – 50th centiles), his height was 115 cm (3rd centile), and his weight was 22 kg (10th centile). The phenotype was remarkable for strabismus, a high hairline, and a thin upper lip. Array-SNP analysis revealed normal results.

Proband's mother (II-2)

The mother of the proband was healthy and had no minor facial anomalies. The stature of the mother was normal, with no abnormalities of the extremities. Her second pregnancy ended with a spontaneous abortion after 5 weeks of gestation.

Proband's father (II-1)

The father was healthy, according to the mother of the patient.

Proband's affected brother (III-3)

The newborn from the mother's 3rd pregnancy, a male, had multiple congenital anomalies, including diaphragmatic hernia, cryptorchidism, and a single umbilical artery. He died 5 weeks after birth.

The clinical features of the proband and his affected brother were consistent with a clinical diagnosis of Tønne-Kalscheuer syndrome.

Genetic testing and protein structure analysis

To detect the disease-causing variant, high-throughput whole-exome sequencing analysis was performed. A hemizygous missense variant NM_016120.4:c.1721T >A, NP_057204.2:p.(Ile574Asn) located in the *RLIM* gene was identified in the proband's gDNA sample after analysis of WES data. There were no pathogenic variants in other genes such as *PIGN*, *LRP2*, *STRA6*, *GPC3*, *CHD7*, or *NIPBL*. This variant has not been previously reported in the literature and was not found in the ExAC [33], GnomAD [34], 1000 Genome Project [35], NCBI dbSNP [36], or NCBI ClinVar [37] databases. In silico analysis with Sift [38] (score 0) and PolyPhen-2 [39] (score 0.997) classified this variant as pathogenic or most probably damaging. The CADD [40] score of the variant is 25.8. AlphaMissense [32] predicted the variant as pathogenic (0.9992) [32]. The variant of interest had high conservation scores (GERP + + 4.21, phyloP100 8.891). A comparative sequence alignment of the RLIM protein across evolutionarily distant species confirmed that the missense variant detected in our proband affects an evolutionarily conserved region (Fig. 1B).

Validation and segregation analysis performed by Sanger sequencing confirmed the asymptomatic mother as a carrier of a familial variant. The variant was not detected in the proband's healthy brother. Other family members were not available for genetic testing.

A study of the methylation of the AR gene was performed to investigate the X-chromosome inactivation (XCI) pattern. In the proband's gDNA, the tested allele was not methylated and was therefore degraded after HpaII digestion. In control females, the XCI ratio was 53:47, showing a random XCI pattern. The amplification of tested alleles of the mother's digested gDNA was markedly deviated, showing a highly skewed (> 95%) XCI pattern. The AR allele with 24 CAG repeats (amplicon size 277 nt) carried in the X chromosome is predominantly inactive (Supplementary Fig. S1). Analysis of fragments of amplified, undigested DNA revealed that the proband's mutated AR allele has 24 CAG repeats (amplicon size 277 nt). Thus, the X chromosome with the RLIM variant is predominantly inactive in the mother.

To estimate the effect of the missense variant on protein structure and function, computational analysis of available structural data was performed. Human RLIM/

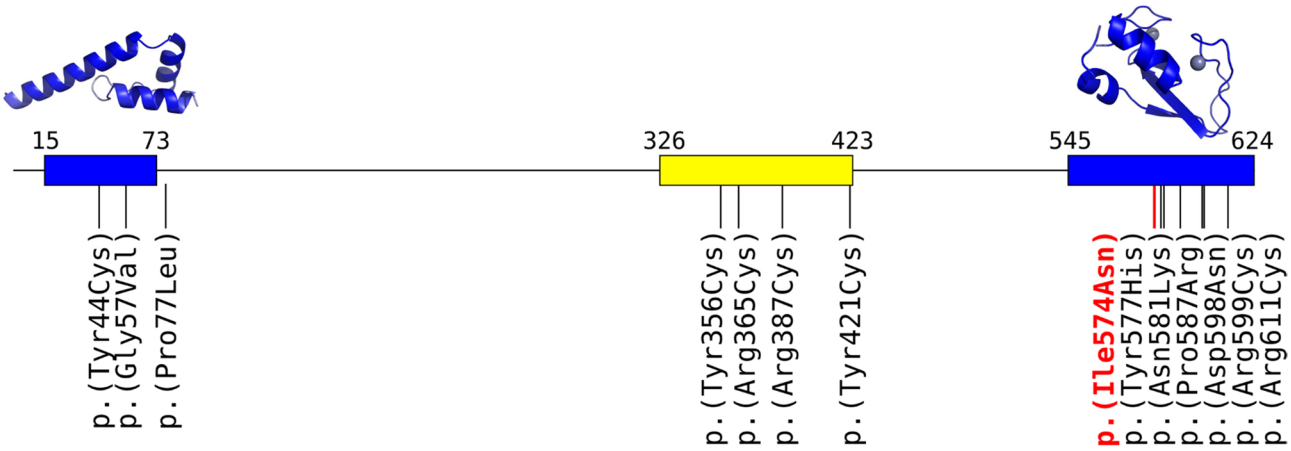

Fig. 2 Schematic representation of the human RLIM protein with known disease-causing variants to date. Regions that are predicted with high reliability (pLDDT >70) in the AlphaFold Database model are highlighted in blue: three alpha-helices in the N-terminus and RING-H2 zinc finger domain in the C-terminus. The basic region necessary for chromatin recruitment [42] is highlighted in yellow

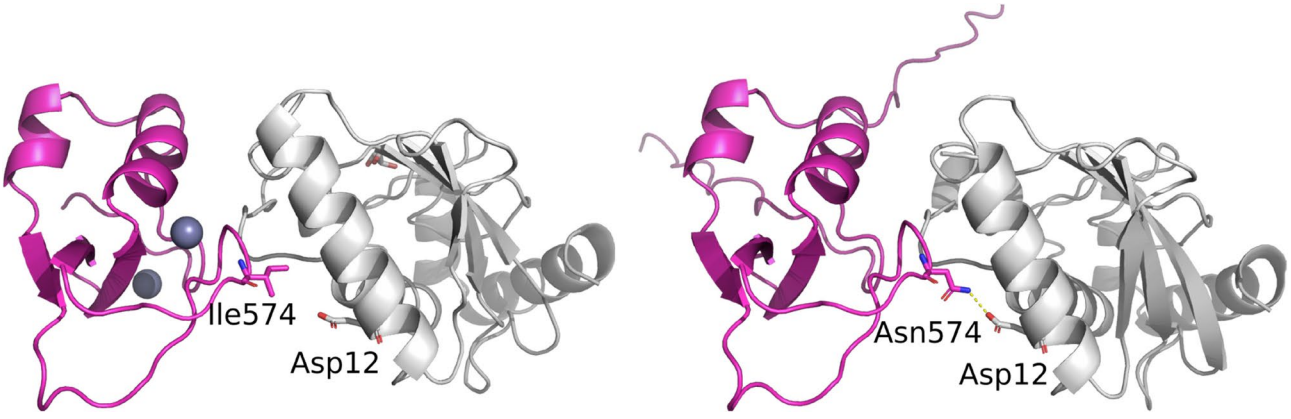

Fig. 3 Experimental structure of the RING-H2 domain of human E3 ubiquitin ligase RLIM (magenta) complex with E2 ubiquitin conjugating enzyme UBE2D2 (grey) (PDB: 6W7Z, left) and AlphaFold model of RLIM_Ile574Asn-UBE2D2 interaction (right) showing an additional hydrogen formed between Asn574 of E3 and Asp12 of E2

RNF12 consists of 624 amino acids. Both AlphaFold and DISOPRED3 predicted the protein to be mostly disordered. In the AlphaFold Database model, only two parts of the structure are predicted with high reliability (pLDDT >70): three alpha-helices in the N-terminus, and the RING-H2 zinc finger domain at the C-terminus (Fig. 2). The C-terminal catalytic RING-H2 zinc finger domain is critical for binding E2 ubiquitin-conjugating proteins [41]. A conserved basic region, adjacent to the RING domain (residues 326–423), is critical for RLIM recruitment to chromatin and RLIM-dependent gene regulation [42].

Experimental structures are known for the RING domain and its interactions with the E2 ubiquitin-conjugating enzymes [41], and the affected residue Ile574 is at the interaction interface in these structures (PDB: 6W7Z, 6W9A, 9W9D). This large hydrophobic residue mostly interacts with hydrophilic residues (Arg, Lys, Glu, Asp, and Thr) from the E2 protein. Moreover, in human E2 enzymes, the binding site residues are highly conserved among the RLIM-interacting UBE2D and UBE2E families, but not in other E2 proteins [28] (Supplementary Fig. S2). The high degree of binding site conservation suggests that even minor changes of the RLIM interacting surface residues might have a significant influence on protein-protein binding. This is consistent with AlphaMissense [32] predictions, where almost all substitutions of the E3–E2 interface residues are predicted to be pathogenic. According to the AlphaFold models, the variant p.(Ile574Asn) may lead to additional hydrogen bonds between RLIM and E2 enzymes, which could significantly alter the E3-E2 interaction (Fig. 3), possibly resulting in further effects on regulatory pathways. Thus, alterations of the ubiquitin-mediated protein degradation pathway might be predicted to be the leading pathomechanism of Tønne-Kalscheuer syndrome in our proband.

Based on the findings of our study and the criteria provided by ACMG [15], the c.1721T >A variant was classified as likely pathogenic (PM1, PM2, PP2, PP3, PP4) and resulting in Tønne-Kalscheuer syndrome.

Discussion

Thus far, 13 variants associated with Tønne-Kalscheuer syndrome in nearly 20 unrelated families have been reported [3, 5–9]. Most of them were located within exon 4 of the *RLIM* gene and altered RLIM putative basic binding domain (e.g., p.(Tyr356Cys), p.(Arg365Cys), p.(Arg387Cys), p.(Tyr421Cys)) or of the C-terminal catalytic RING-H2 zinc finger domain (e.g., p.(Tyr577His), p.(Asn581Lys), p.(Pro587Arg), p.(Asp598Asn), p.(Arg599Cys), p.(Arg611Cys)), except for the substitution p.(Pro77Leu) (Fig. 2). The latter has been detected at a frequency of 0.0003895, including two hemizygotes in the GnomAD [34], and due to conflicting evidence for pathogenicity this family was not included in further discussion in this study. The other two *RLIM* variants, p.(Tyr44Cys) and p.(Gly57Val), located outside the two mutate[4onal hotspots, also resulted in a phenotype consistent with TOKAS [8]. Although less frequent, these variants may still impair protein function by disrupting emerging intramolecular regulatory mechanisms [8].

The RLIM (RNF12) protein belongs to the largest family of ubiquitin E3 ligases and is detected mostly in cell nuclei [43]. E3 ubiquitin ligase has been found to target LIM domain binding 1 (LDB1) and cause its proteasome-dependent degradation. This protein, together with LDB1, functions as a co-repressor of a LIM homeodomain transcription factor, which is crucial for the development of neuronal structures and cellular differentiation [41]. The RLIM protein is also a key regulator in p53 and TGF-β signalling pathways [44, 45]. Some independent studies of mouse models have shown that the ortholog of human *RLIM* acts in the X-chromosome inactivation process by regulation of *Xist* (a long non-coding RNA) expression [4, 46]. Another study of RLIM-deficient embryonic stem cell models demonstrated upregulation of neural lineage markers such as Sox1, Pax6, and Ascl1, as well as the development of neuronal cell morphology and enhanced neurite outgrowth. These findings suggest that RLIM regulates developmental timing during neuronal differentiation, indicating a potential function of RLIM that may be disrupted in XLID [28]. Also, in vivo, functional experiments of knockout zebrafish resulted in microcephaly that is consistent with the human phenotype [6]. The wide spectrum of different functions of the RLIM protein explains its expression in almost all tissues [47].

Although approximately 60 individuals carrying pathogenic *RLIM* variants have been reported to date, comprehensive clinical characterization remains challenging due to the lack of detailed phenotypic data for many affected individuals. Nevertheless, variation in the severity of the disorder within reported families has been seen, with the disorder presenting with either lethal multiple congenital malformation disorders or much milder phenotypes in affected individuals due to possible variable expression of the syndrome. Variants of the C-terminal catalytic RING-H2 zinc finger domain have been suggested to be more deleterious than variants affecting the RLIM binding locus. For example, such severe features as congenital diaphragmatic hernia (CDH) manifested in six previously reported families with pathogenic p.(Tyr44Cys), p.(Gly57Val), p.(Tyr421Cys), p.(Tyr577His), p.(Asp598Asn), and p.(Arg611Cys) variants. These variants, except for the p.(Tyr421Cys) substitution, were located in the C-terminal catalytic RING-H2 zinc finger domain [5, 6]. The affected brother of our proband had a CDH and cryptorchidism, which are characteristic features of the TOKAS. Although the proband's affected brother (III-3) was not tested, specific clinical features suggest a severe manifestation of the novel, likely pathogenic variant p.(Ile574Asn) in *RLIM*. Compared to the proband (III-1), the affected brother's (III-3) phenotype was more severe, supporting the notion that the same RLIM variant may result in variable clinical expression, likely influenced by complex individual-specific modifying mechanisms The proband's mother (II-2), a carrier of the familial p.(Ile574Asn) variant, has a normal phenotype with normal cognitive function and behaviour, likely because of a highly skewed (>95%) XCI pattern (Fig. 1A). Similarly, in the study provided by Frints et al. (2019), all carrier females from reported families demonstrated highly skewed XCI with preferential inactivation of the mutant X chromosome. While the majority of heterozygous females presented with normal cognition and behaviour, a few were noted to have mild physical features, such as skeletal anomalies, suggesting that incomplete skewing or tissue-specific XCI may occasionally contribute to subtle manifestations in carriers [6].

All of the reported pathogenic variants are missense variants, suggesting that complete loss of RLIM function may be incompatible with life in male individuals. The majority of *RLIM* missense variants reported in healthy males, in, e.g., the GnomAD population database [34], are located outside the RLIM putative basic binding domain or the C-terminal catalytic RING-H2 zinc finger domain. Analysis of RLIM structural data shows that known residues in the variants of the RLIM RING-H2 domain are not interacting with Zn. Such a genetic change would probably have critical effects on the structure of the RING-H2 domain, resulting in a total loss of function. Almost all substitutions of residues in the RLIM-E2 enzyme interaction interfaces are predicted to be pathogenic using AlphaMissense [32], indicating the

key role of this region. Among the pathogenic variants described, there are substitutions of several arginine residues at the interface of RLIM interaction with E2 ligases (p.(Arg599Cys), p.(Arg611Cys)). According to the known structures, these mutations could break down hydrogen bonds and salt bridges that are formed with E2 ligases. In contrast, the likely pathogenic variant detected in our proband, p.(Ile574Asn), might form an additional hydrogen bond, possibly making the protein-protein interaction stronger or influencing the binding kinetics. Such a disruption of the E3–E2 interaction is expected to impair downstream protein interactions and regulatory processes. However, elucidation of the precise molecular mechanisms requires further experimental investigation. TOKAS-specific reporters are currently under development and hold promise for advancing our understanding of the pathogenic consequences of RLIM variants [9].

Conclusions

The findings provided in this study suggest that the affected residue p.(Ile574) could alter the interactions of the RING domain with E2 ubiquitin-conjugating enzymes and, therefore, may influence the ubiquitin-mediated protein regulation pathways. While in silico and structural predictions strongly support a functional impact, further experimental functional assays are essential to conclusively demonstrate disruption of E2 interactions. Also, further genotype–phenotype correlations are needed to better understand the inter- and intra-familial variability in clinical expression, which is critical for accurate genetic counselling, timely diagnosis, personalized treatment planning, and improved family support.

Supplementary Information

The online version contains supplementary material available at https://doi.org/10.1186/s12887-025-06194-3.

Supplementary Material 1.

Supplementary Material 2.

Supplementary Material 3.

Supplementary Material 4.

Acknowledgements

We thank the family and control individuals for participating in this study. Also, we are grateful to the personnel at CeGaT GmbH, Tübingen, Germany, for technical assistance.

Authors' contributions

Conceptualization, E.P.; data curation, E.S., J.D., Ž.M., V.M., G.P., and E.P.; formal analysis, E.S., J.D., Ž.M., V.M., G.P., and E.P.; funding acquisition, E.P.; investigation, Ž.M. and V.M.; project administration, E.P; software, E.S., Ž.M., V.M., and J.D.; supervision, E.P.; validation, Ž.M., V.M., and E.P.; visualization, E.S., J.D., and E.P.; writing—original draft, E.S., J.D., and E.P.; writing—review and editing, E.S., J.D., Ž.M., V.M., G.P., and E.P. All authors have read and agreed to the published version of the manuscript.

Funding

This study was funded by a grant (No. S-MIP-21-15; ATGC project) from the Research Council of Lithuania. The funders had no role in the design of the study, data collection and analysis, preparation of the manuscript, or the decision to publish.

Data availability

The datasets generated and analysed during the current study are available in the Zenodo repository (https://doi.org/10.5281/zenodo.13256061).

Declarations

Ethics approval and consent to participate

Informed consent for genetic testing in the context of clinical care and diagnosis, as well as for participation in this study and for publication, was obtained from the parents at the Centre for Medical Genetics, Vilnius Hospital Santaros Klinikos. This research was conducted according to the guidelines of the Declaration of Helsinki and approved by the Vilnius Regional Biomedical Research Ethics Committee of Lithuania (protocol code No. 2021/9-1373-849, date of approval 21 September 2021).

Competing interests

The authors declare no competing interests.

Received: 17 July 2024 / Accepted: 15 September 2025
Published online: 09 October 2025

References

1. Schwartz CE, Louie RJ, Toutain A, Skinner C, Friez MJ, Stevenson RE. X-linked intellectual disability update 2022. Am J Med Genet Part A. 2023;191:144–59.
2. Ilyas M, Mir A, Efthymiou S, Houlden H. The genetics of intellectual disability: advancing technology and gene editing. F1000Res. 2020. https://doi.org/10.12688/f1000research.16315.1.
3. Tønne E, Holdhus R, Stansberg C, Stray-Pedersen A, Petersen K, Brunner HG, et al. Syndromic X-linked intellectual disability segregating with a missense variant in RLIM. Eur J Hum Genet. 2015;23:1652–6.
4. Hu H, Haas SA, Chelly J, Van Esch H, Raynaud M, de Brouwer APM, et al. X-exome sequencing of 405 unresolved families identifies seven novel intellectual disability genes. Mol Psychiatry. 2016;21:133–48.
5. Bustos F, Espejo-Serrano C, Segarra-Fas A, Toth R, Eaton AJ, Kernohan KD, et al. A novel RLIM/RNF12 variant disrupts protein stability and function to cause severe Tonne-Kalscheuer syndrome. Sci Rep. 2021;11:9560.
6. Frints SGM, Ozanturk A, Rodríguez Criado G, Grasshoff U, de Hoon B, Field M, et al. Pathogenic variants in E3 ubiquitin ligase RLIM/RNF12 lead to a syndromic x-linked intellectual disability and behavior disorder. Mol Psychiatry. 2019;24:1748–68.
7. Templeton KM, Thompson L, Tobias ES, Ahmed SF, McGowan R. Coloboma in a family with Tonne-Kalsheuer syndrome: extending the phenotype of RLIM variants. Clin Dysmorphol. 2024;33:38–42.
8. Cuinat S, Quélin C, Effray C, Dubourg C, Le Bouar G, Cabaret-Dufour A-S, et al. Extending the clinical spectrum of X-linked Tonne-Kalscheuer syndrome (TOKAS): new insights from the fetal perspective. J Med Genet. 2024;61:824–32.
9. Bandi V, Rennie M, Koch I, Gill P, Pacheco OD, Berg AD, et al. RLIM-specific activity reporters define variant pathogenicity in Tonne-Kalscheuer syndrome. Hum Genet Genomics Adv. 2025. https://doi.org/10.1016/j.xhgg.2024.100378.
10. Siavrienė E, Maldžienė Ž, Mikštienė V, Petraitytė G, Rančelis T, Dapkūnas J, et al. PIGN-related disease in two Lithuanian families: a report of two novel pathogenic variants, molecular and clinical characterisation. Medicina (Kaunas). 2022;58:1526.
11. Javadi A, Shamaei M, Ziazi LM, Pourabdollah M, Dorudinia A, Seyedmehdi SM, et al. Qualification study of two genomic DNA extraction methods in different clinical samples. Tanaffos. 2014;13:41–7.
12. Jiang H, Lei R, Ding S-W, Zhu S. Skewer: a fast and accurate adapter trimmer for next-generation sequencing paired-end reads. BMC Bioinformatics. 2014;15:182.
13. Li H, Durbin R. Fast and accurate short read alignment with Burrows-Wheeler transform. Bioinformatics. 2009;25:1754–60.

14. Wang K, Li M, Hakonarson H. ANNOVAR: functional annotation of genetic variants from high-throughput sequencing data. Nucleic Acids Res. 2010;38:e164–164.
15. Richards S, Aziz N, Bale S, Bick D, Das S, Gastier-Foster J, et al. Standards and guidelines for the interpretation of sequence variants: a joint consensus recommendation of the American college of medical genetics and genomics and the association for molecular pathology. Genet Med. 2015;17:405–23.
16. Robinson JT, Thorvaldsdóttir H, Winckler W, Guttman M, Lander ES, Getz G, et al. Integrative genomics viewer. Nat Biotechnol. 2011;29:24–6.
17. Allen RC, Zoghbi HY, Moseley AB, Rosenblatt HM, Belmont JW. Methylation of Hpall and Hhal sites near the polymorphic CAG repeat in the human androgen-receptor gene correlates with X chromosome inactivation. Am J Hum Genet. 1992;51:1229–39.
18. Bertelsen B, Tümer Z, Ravn K. Three new loci for determining x chromosome inactivation patterns. J Mol Diagn. 2011;13:537–40.
19. Bateman A, Martin M-J, Orchard S, Magrane M, Ahmad S, Alpi E, et al. UniProt: the universal protein knowledgebase in 2023. Nucleic Acids Res. 2023;51:D523–31.
20. Varadi M, Anyango S, Deshpande M, Nair S, Natassia C, Yordanova G, et al. AlphaFold protein structure database: massively expanding the structural coverage of protein-sequence space with high-accuracy models. Nucleic Acids Res. 2022;50:D439–44.
21. Dapkūnas J, Timinskas A, Olechnovič K, Tomkuvienė M, Venclovas Č. PPI3D: a web server for searching, analyzing and modeling protein-protein, protein-peptide and protein-nucleic acid interactions. Nucleic Acids Res. 2024;52:W264–71.
22. Jumper J, Evans R, Pritzel A, Green T, Figurnov M, Ronneberger O, et al. Highly accurate protein structure prediction with alphafold. Nature. 2021;596:583–9.
23. Evans R, O'Neill M, Pritzel A, Antropova N, Senior A, Green T, et al. Protein complex prediction with AlphaFold-Multimer. BioRxiv. 2022;1-25. https://doi.org/10.1101/2021.10.04.463034
24. Olechnovič K, Venclovas Č, Voronota A. A fast and reliable tool for computing the vertices of the Voronoi diagram of atomic balls. J Comput Chem. 2014;35:672–81.
25. McDonald IK, Thornton JM. Satisfying hydrogen bonding potential in proteins. J Mol Biol. 1994;238:777–93.
26. Olechnovič K, Venclovas Č. VoroContacts: a tool for the analysis of interatomic contacts in macromolecular structures. Bioinformatics. 2021;37:4873–5.
27. Jones DT, Cozzetto D. DISOPRED3: precise disordered region predictions with annotated protein-binding activity. Bioinformatics. 2015;31:857–63.
28. Bustos F, Segarra-Fas A, Chaugule VK, Brandenburg L, Branigan E, Toth R, et al. RNF12 x-linked intellectual disability mutations disrupt E3 ligase activity and neural differentiation. Cell Rep. 2018;23:1599–611.
29. Katoh K, Standley DM. MAFFT multiple sequence alignment software version 7: improvements in performance and usability. Mol Biol Evol. 2013;30:772–80.
30. Waterhouse AM, Procter JB, Martin DMA, Clamp M, Barton GJ. Jalview version 2—a multiple sequence alignment editor and analysis workbench. Bioinformatics. 2009;25:1189–91.
31. Crooks GE, Hon G, Chandonia JM, Brenner SE. Weblogo: a sequence logo generator. Genome Res. 2004;14:1188–90.
32. Cheng J, Novati G, Pan J, Bycroft C, Žemgulytė A, Applebaum T, et al. Accurate proteome-wide missense variant effect prediction with alphamissense. Science. 2023. https://doi.org/10.1126/science.adg7492.
33. Karczewski KJ, Weisburd B, Thomas B, Solomonson M, Ruderfer DM, Kavanagh D, et al. The ExAC browser: displaying reference data information from over 60 000 exomes. Nucleic Acids Res. 2017;45:D840–5.
34. Karczewski KJ, Francioli LC, Tiao G, Cummings BB, Alföldi J, Wang Q, et al. The mutational constraint spectrum quantified from variation in 141,456 humans. Nature. 2020;581:434–43.
35. 1000 Genomes Project Consortium, Auton A, Brooks LD, Durbin RM, Garrison EP, Kang HM, et al. A global reference for human genetic variation. Nature. 2015;526:68–74.
36. Sherry ST. DbSNP: the NCBI database of genetic variation. Nucleic Acids Res. 2001;29:308–11.
37. Landrum MJ, Lee JM, Riley GR, Jang W, Rubinstein WS, Church DM, et al. ClinVar: public archive of relationships among sequence variation and human phenotype. Nucleic Acids Res. 2014;42:D980–5.
38. Sim NL, Kumar P, Hu J, Henikoff S, Schneider G, Ng PC. Sift web server: predicting effects of amino acid substitutions on proteins. Nucleic Acids Res. 2012;40:W452-7.
39. Miosge LA, Field MA, Sontani Y, Cho V, Johnson S, Palkova A, et al. Comparison of predicted and actual consequences of missense mutations. Proc Natl Acad Sci U S A. 2015;112:E5189-98.
40. Rentzsch P, Witten D, Cooper GM, Shendure J, Kircher M. CADD: predicting the deleteriousness of variants throughout the human genome. Nucleic Acids Res. 2019;47:D886–94.
41. Middleton AJ, Zhu J, Day CL. The RING domain of RING finger 12 efficiently builds degradative ubiquitin chains. J Mol Biol. 2020;432:3790–801.
42. Espejo-Serrano C, Aitken C, Tan BF, May DG, Chrisopulos RJ, Roux KJ, et al. Chromatin targeting of the RNF12/RLIM E3 ubiquitin ligase controls transcriptional responses. Life Sci Alliance. 2024. https://doi.org/10.26508/lsa.202302282.
43. Wang F, Bach I. Rlim/Rnf12, Rex1, and X chromosome inactivation. Front Cell Dev Biol. 2019;7:258.
44. Gao K, Wang C, Jin X, Xiao J, Zhang E, Yang X, et al. RNF12 promotes p53-dependent cell growth suppression and apoptosis by targeting MDM2 for destruction. Cancer Lett. 2016;375:133–41.
45. Zhang L, Huang H, Zhou F, Schimmel J, Pardo CG, Zhang T, et al. RNF12 controls embryonic stem cell fate and morphogenesis in zebrafish embryos by targeting Smad7 for degradation. Mol Cell. 2012;46(5):650–61.
46. Shin J, Wallingford MC, Gallant J, Marcho C, Jiao B, Byron M, et al. Rlim is dispensable for X-chromosome inactivation in the mouse embryonic epiblast. Nature. 2014;511:86–9.
47. Rivas MA, Pirinen M, Conrad DF, Lek M, Tsang EK, Karczewski KJ, et al. Effect of predicted protein-truncating genetic variants on the human transcriptome. Science. 2015;348:666–9.

Publisher's Note